arXiv:1602.02328v2 [cond-mat.quant-gas] 12 May 2016

Path integral Monte Carlo determination of the fourth-order virial coefficient for unitary two-component Fermi gas with zero-range interactions

Yangqian Yan[1] and D. Blume[1]

[1] *Department of Physics and Astronomy, Washington State University, Pullman, Washington 99164-2814, USA*

(Dated: May 13, 2016)

The unitary equal-mass Fermi gas with zero-range interactions constitutes a paradigmatic model system that is relevant to atomic, condensed matter, nuclear, particle, and astro physics. This work determines the fourth-order virial coefficient b_4 of such a strongly-interacting Fermi gas using a customized *ab initio* path integral Monte Carlo (PIMC) algorithm. In contrast to earlier theoretical results, which disagreed on the sign and magnitude of b_4, our b_4 agrees within error bars with the experimentally determined value, thereby resolving an ongoing literature debate. Utilizing a trap regulator, our PIMC approach determines the fourth-order virial coefficient by directly sampling the partition function. An on-the-fly anti-symmetrization avoids the Thomas collapse and, combined with the use of the exact two-body zero-range propagator, establishes an efficient general means to treat small Fermi systems with zero-range interactions.

PACS numbers: 03.75.-b

Introduction: Strongly-interacting Fermi gases manifest themselves in nature in different forms, from neutrons in neutron stars [1] to electrons in solids [2]. These systems are generally deemed difficult to treat theoretically because of the lack of a small interaction parameter. Superconductivity [3] and exotic states such as fractional quantum hall [4] or Fulde-Ferrell-Larkin-Ovchinnikov [5–7] states have been observed or predicted to exist in these systems. Ultracold Fermi gases [8, 9], which can nowadays be produced routinely in table-top experiments, are ideal for studying strongly-interacting systems since (i) the van der Waals interaction is short-ranged, which means that it can be approximated by a contact potential that introduces a single length scale, i.e., the s-wave scattering length a_s; and (ii) a_s can be tuned at will utilizing Feshbach resonance techniques [10]. When a_s diverges, i.e., becomes infinitely large, the two-body contact potential does not define a length scale [11]. Just like the non-interacting Fermi gas, the properties of the unitary Fermi gas (Fermi gas with infinite a_s) are determined by two length scales, the de Broglie wavelength λ and interparticle spacing $\bar{r}$ [12].

At high temperature, λ is much smaller than $\bar{r}$ and the grand canonical thermodynamic potential Ω can be expanded in terms of the fugacity [13, 14]. The n^{th}-order expansion or virial coefficient b_n is determined by the partition functions of clusters containing n or fewer fermions. Since all thermodynamic properties at high temperature can be derived from the virial coefficients b_n [15], the b_n's are essential to understanding the normal state of strongly-interacting Fermi gases.

While the second- and third-order virial coefficients are well understood [13, 15–21], none of the theoretical calculations for b_4 [22–25] agree with the experimental data [19, 26]. This letter rectifies this situation: our theoretically determined b_4 agrees with the experimentally determined value. Our approach uses a trap regulator [27, 28] and employs the path integral Monte Carlo (PIMC) technique [29, 30], with the contact interactions incorporated exactly via the two-body zero-range propagator [31]. The "post-anti-symmetrization" [29, 30], traditionally employed in PIMC calculations, does not work for the system with zero-range interactions, since the sampled paths shrink due to the Thomas collapse, a well known phenomenon for bosons [32, 33], to a single point. For bosons, the three-body Thomas collapse is cured by introducing an additional scale or three-body parameter [33]. For fermions, such a three-body parameter is not needed since the Pauli exclusion principle acts as an effective three-body repulsion [34, 35]. Thus, rather than the standard "post-anti-symmetrization", we use an "on-the-fly scheme" [36, 37], which anti-symmetrizes at each imaginary time step. While the anti-symmetrization is, within Monte Carlo frameworks, usually associated with the infamous Fermi sign problem [38–40], in our case it stabilizes the simulation and affords the use of significantly smaller number of time slices than the use of finite-range interactions would. Our approach reproduces the trap regulated b_3 over a wide temperature range. We determine the trap regulated b_4 as a function of the temperature T. In the low-temperature regime, we find agreement with Ref. [22]. We separate the spin-balanced ($b_{2,2}/2$) and spin-imbalanced ($b_{3,1}$) sub-cluster contributions to b_4, $b_4 = b_{3,1} + b_{2,2}/2$, and find $b_{2,2} < 0$ and $b_{3,1} > 0$ at all considered temperatures. $b_{2,2}$ dominates at low T and $b_{3,1}$ at high T. Converting the trap regulated virial coefficient b_4 to that of the homogeneous system using the local density approximation (LDA) [16], we find agreement with the experimentally determined values [19, 26].

Virial expansion framework: The n^{th}-order virial coefficient b_n^{hom} of the homogeneous system at unitarity is related to the high-temperature limit b_n^0 of the harmonically trapped unitary system via $b_n^{\text{hom}} = n^{3/2} b_n^0$ [16, 28]. To determine b_n^0, we calculate the virial coefficient b_n of the harmonically trapped system for various temperatures and then take the $T \to \infty$ limit. The trap Hamiltonian $H(n_1, n_2)$ for n_1 particles of species 1 and n_2 par-

ticles of species 2 with interspecies s-wave interactions reads

$$H(n_1,n_2) = \sum_{j=1}^{n_1+n_2}\left(\frac{-\hbar^2}{2m}\nabla^2_{\mathbf{r}_j} + \frac{1}{2}m\omega^2\mathbf{r}_j^2\right) + \sum_{i=1}^{n_1}\sum_{j=n_1+1}^{n_1+n_2} V_{2b}(\mathbf{r}_i-\mathbf{r}_j), \quad (1)$$

where m denotes the mass of the particles, $\mathbf{r}_j$ the position vector of the j^{th} particle, ω the angular trapping frequency, and V_{2b} the regularized Fermi-Huang pseudopotential with infinite a_s [41]. The grand canonical thermodynamic potential Ω can be written in terms of the fugacities z_i of species i,

$$\Omega = -k_BT\ln\left(\sum_{n_1=0}^{\infty}\sum_{n_2=0}^{\infty} Q_{n_1,n_2} z_1^{n_1} z_2^{n_2}\right), \quad (2)$$

where z_i is equal to $\exp[\mu_i/(k_BT)]$, μ_i is the chemical potential of species i, and Q_{n_1,n_2} is the canonical partition function for $H(n_1,n_2)$,

$$Q_{n_1,n_2} = \text{ Tr } \exp\left[-H(n_1,n_2)/(k_BT)\right]. \quad (3)$$

Here, Tr is the trace operator. Defining $\Delta\Omega = \Omega - \Omega^{\text{ni}}$, where Ω^{ni} is the grand canonical potential of the non-interacting system, and Taylor-expanding around $z_1 = z_2 = 0$ [42, 43], one finds

$$\Delta\Omega = -k_BTQ_{1,0}\left(\sum_{n_1=1}^{\infty}\sum_{n_2=1}^{\infty} b_{n_1,n_2} z_1^{n_1} z_2^{n_2}\right). \quad (4)$$

For spin-balanced systems, z_1 and z_2 are equal and Eq. (4) reduces to

$$\Delta\Omega = -2k_BTQ_{1,0}\left(\sum_{n=2}^{\infty} b_n z^n\right), \quad (5)$$

where $b_2 = b_{1,1}/2$, $b_3 = (b_{1,2}+b_{2,1})/2$, and $b_4 = (b_{1,3}+b_{3,1}+b_{2,2})/2$ (note, one has $b_{2,1} = b_{1,2}$ and $b_{3,1} = b_{1,3}$). It is convenient to write the virial coefficients b_{n_1,n_2} as

$$b_{n_1,n_2} = \Delta b_{n_1,n_2} + b^{\text{ref}}_{n_1,n_2}, \quad (6)$$

where $b^{\text{ref}}_{n_1,n_2}$ is determined by the virial coefficients b_{j_1,j_2} and the canonical partition functions Q_{j_1,j_2} with $j_1+j_2 < n_1+n_2$. The term $\Delta b_{n_1,n_2} = (Q_{n_1,n_2} - Q^{\text{ni}}_{n_1,n_2})/Q_{1,0}$, where $Q^{\text{ni}}_{n_1,n_2} = Q_{n_1,0}Q_{0,n_2}$, in contrast, accounts for the "new" physics introduced by the interacting (n_1,n_2) clusters [44].

Contradicting literature results for b_4: The literature results are summarized in Table I (see also the supplemental material [45]). Two independent experiments find consistent values for the fourth-order virial coefficient. The theoretical literature results, however, disagree with these experimental results, reflecting the fact that the fourth-order problem is highly non-trivial analytically and numerically. Using a sum-over-states approach with an energy cutoff, Ref. [22] obtained the low-temperature behavior of b_4. Assuming a monotonic temperature dependence and extrapolating to the $T\to\infty$ limit, Ref. [22] obtained b_4^0. It was concluded that more four-body energies would need to be calculated explicitly to obtain b_4 reliably at high temperature. The fourth-order virial coefficient has also been obtained by a diagrammatic approach, which included only a subset of the four-body free-space diagrams [23], and by applying a conjecture inspired by three-body results [24, 25].

Customized PIMC algorithm: $\Delta b_{n_1,n_2}$ is determined by the partition function Q_{n_1,n_2} of the interacting (n_1,n_2) system (Q_{n_1,n_2} is not known in general) and the partition function $Q^{\text{ni}}_{n_1,n_2}$ of the non-interacting (n_1,n_2) system ($Q^{\text{ni}}_{n_1,n_2}$ is known analytically). We calculate the ratio of the partition functions $Q^{\text{ni}}_{n_1,n_2}/Q_{n_1,n_2}$ using the PIMC technique. Specifically, the simulation generates configurations according to Q_{n_1,n_2} and accumulates the ratio $Q^{\text{ni}}_{n_1,n_2}/Q_{n_1,n_2}$ as a weight. The reason for using the partition function of the unitary Fermi gas and not that of the non-interacting gas as the "guiding function" is the following. The probability density to find two unlike particles with vanishing interparticle spacing is finite at unitarity and zero in the non-interacting limit. If we used $Q^{\text{ni}}_{n_1,n_2}$ as the guiding function, configurations in which two unlike particles are at the same spatial position would be absent and the standard deviation of $Q_{n_1,n_2}/Q^{\text{ni}}_{n_1,n_2}$ would be infinite, rendering the expectation value meaningless [46].

In the PIMC formulation, the partition function $Q^{\text{boltz}}_{n_1,n_2}(\beta)$ for Boltzmann particles (no exchange symmetries) at inverse temperature β, $\beta = (k_BT)^{-1}$, is written in terms of a product over density matrices at imaginary time τ,

$$Q^{\text{boltz}}_{n_1,n_2}(\beta) = \int\ldots\int\prod_{i=1}^{N}\rho(\mathbf{R}_i,\mathbf{R}_{i+1};\tau)d\mathbf{R}_1\ldots d\mathbf{R}_N, \quad (7)$$

where $\mathbf{R}_i$ collectively denotes the particle configurations at time slice i, $\mathbf{R}_N = \mathbf{R}_1$, and $N = \beta/\tau$. For the two-component Fermi gas, the standard PIMC approach writes the partition function as $Q_{n_1,n_2} = \mathcal{A}Q^{\text{boltz}}_{n_1,n_2}$, where $\mathcal{A}$ is the anti-symmetrizer [29, 47]. For the two-component Bose gas, the anti-symmetrizer $\mathcal{A}$ is replaced by the symmetrizer $\mathcal{S}$. $\mathcal{A}$ and $\mathcal{S}$ contain the same number and types of terms; however, while all terms in $\mathcal{S}$ enter

TABLE I. Summary of literature and PIMC results.

b_4^{hom}	b_4^0	Ref.	comment
0.096(15)	0.01200(188)	[19]	ENS experiment
0.096(10)	0.01203(125)	[26]	MIT experiment
−0.016(4)	−0.0020(5)	[22]	sum-over-states approach
0.06	0.0075	[23]	diagrammatic approach
−0.063(1)	−0.007875(125)	[24]	3-body inspired conjecture
0.078(18)	0.0098(23)		PIMC, this work

with a plus sign, $\mathcal{A}$ contains alternating plus and minus signs. Since the symmetrizer and anti-symmetrizer are, in the standard PIMC approach, evaluated stochastically, the two-component Fermi and Bose gases are simulated using the same paths. Expectation values, however, are accumulated with plus and minus signs for fermions and with plus signs only for bosons. We refer to this standard approach as post-symmetrization. The bosonic system with interspecies two-body zero-range interactions but without a three-body regulator would collapse to a single point; this is the well-known Thomas collapse [32]. Correspondingly, the fermionic paths would also collapse, rendering the simulation meaningless. To get around this problem, we developed a customized on-the-fly anti-symmetrization scheme, which explicitly anti-symmetrizes the density matrix at each imaginary time step,

$$Q_{n_1,n_2}(\beta) = \int \dots \int \prod_{i=1}^{N} \mathcal{A}\rho(\mathbf{R}_i, \mathbf{R}_{i+1}; \tau) d\mathbf{R}_1 \dots d\mathbf{R}_N. \tag{8}$$

The observable is then calculated using

$$\frac{Q^{\rm ni}_{n_1,n_2}}{Q_{n_1,n_2}} = \left\langle \prod_{i=1}^{N} \frac{\mathcal{A}\rho^{\rm ni}(\mathbf{R}_i, \mathbf{R}_{i+1}; \tau)}{\mathcal{A}\rho(\mathbf{R}_i, \mathbf{R}_{i+1}; \tau)} \right\rangle, \tag{9}$$

where $\rho^{\rm ni}$ denotes the density matrix for the non-interacting system and $\langle \dots \rangle$ the thermal average using paths generated for the unitary Fermi gas using the on-the-fly anti-symmetrization scheme. Our simulation uses the pair-product approximation [29, 45] with the exact two-body density matrix for zero-range interactions. The on-the-fly scheme employed here is related to earlier works [36, 48], which anti-symmetrized, as we do, at each time slice. The key difference is that we employ a density matrix that accounts for the interactions while the earlier works employed the non-interacting density matrix together with the Trotter (or improved Trotter) formula.

The on-the-fly anti-symmetrization scheme treats the $n_1!n_2!$ permutations explicitly at each time slice, eliminating the need of the standard stochastic "permute move". As a consequence, the scheme is computationally prohibitively demanding for large systems. For small systems, however, it is quite efficient for three reasons: (i) The number of permutations is manageable for small $n_1 + n_2$. (ii) The use of the zero-range interactions eliminates the need to perform calculations for several different ranges of the underlying two-body potential. (iii) Compared to finite-range interactions [49], the number of time slices needed to reach convergence for the zero-range interacting systems considered here is rather small; e.g., our scheme yields $Q^{\rm ni}_{3,1}/Q_{3,1}$ at $E_{\rm ho}/(k_BT) = 0.8$ with 0.1% error using only $N = 9$ imaginary time slices (here, $E_{\rm ho} = \hbar\omega$). Within our approach, the key challenge in determining b_4 reliably at high temperature comes from the fact that $\Delta b_{2,2}$, $\Delta b_{3,1}$, $b^{\rm ref}_{2,2}$, and $b^{\rm ref}_{3,1}$ diverge, to leading order, as $(k_BT/E_{\rm ho})^6$. This implies that $b_{2,2}$ and $b_{3,1}$ are, at high temperature, obtained by adding two numbers of opposite sign and nearly equal magnitude. Thus, to obtain reliable values at high temperature, we need to determine our observables with high accuracy. In practice, our available computer time limits us to $k_BT \leq 2E_{\rm ho}$ for the (2,2) and (3,1) systems.

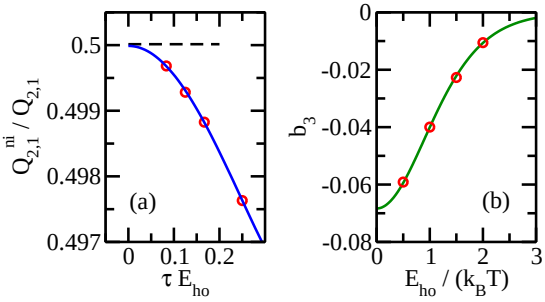

FIG. 1. (Color online) Benchmarking our PIMC results (circles) for the (2,1) system at unitarity through comparison with sum-over-states results. (a) The observable $Q^{\rm ni}_{2,1}/Q_{2,1}$ as a function of the imaginary time step τ at $k_BT = E_{\rm ho}$. The circles show our PIMC results. The error bars (not shown) are smaller than the symbol size. The solid line shows the fourth-order polynomial fit of the form $a + b\tau^2 + c\tau^4$. The dashed line shows the sum-over-states results. (b) b_3 as a function of $1/(k_BT)$. The circles show our PIMC results while the solid line shows the sum-over-states results.

PIMC results: To benchmark our customized PIMC algorithm, we apply it to the (2,1) system at unitarity, for which $Q^{\rm ni}_{2,1}/Q_{2,1}$ and b_3 can be calculated with high accuracy for all temperatures using the sum-over-states approach [16]. As an example, circles in Fig. 1(a) show the quantity $Q^{\rm ni}_{2,1}/Q_{2,1}$ for $k_BT = E_{\rm ho}$, obtained using our PIMC algorithm, as a function of the imaginary time step τ. The τ considered correspond to between $N = 4$ and 10 time slices. The simulation is exact in the $\tau \to 0$ (or equivalently, $N \to \infty$) limit. To extrapolate to the $\tau \to 0$ limit, we fit a fourth-order polynomial of the form $a + b\tau^2 + c\tau^4$ to the PIMC data [solid line in Fig. 1(a)]. Our extrapolated result of 0.499989(26) agrees within error bars with the value of 0.500014 [dashed line in Fig. 1(a)] obtained by the sum-over-states approach. Using the extrapolated $\tau \to 0$ values for $Q^{\rm ni}_{2,1}/Q_{2,1}$ at various temperatures T, we obtain b_3 as a function of T [circles in Fig. 1(b)]. The agreement with the sum-over-states results [solid line in Fig. 1(b)] is excellent for all T considered, demonstrating the reliability and accuracy of our PIMC approach.

We now discuss the determination of b_4. The extrapolation of the raw data to the $\tau \to 0$ limit is discussed in the supplemental material [45]. Circles in Figs. 2(a) and 2(b) show our PIMC results for $b_{3,1}$ and $b_{2,2}$, respectively, as a function of the inverse temperature. At low temperature, the PIMC results agree with the sum-over-states results (solid lines), obtained using the data provided in Ref. [22]. At all temperatures, $b_{3,1}$ is positive and $b_{2,2}$ is negative. It has been shown that $b_{1,1}$

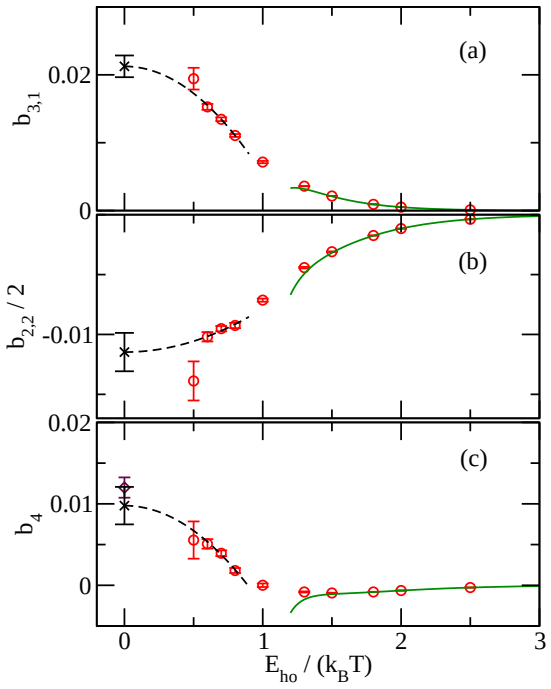

FIG. 2. (Color online) PIMC determination of the fourth-order virial coefficient. Circles in panels (a), (b), and (c) show $b_{3,1}$, $b_{2,2}/2$, and b_4, respectively, determined by our PIMC approach. The crosses in (a) and (b) show the $T \to \infty$ limit of the two-parameter fit (dashed line) to the PIMC data at the four highest temperatures. The dashed line and the cross in (c) show the sum of the fits from (a) and (b). The error bar in (c) is obtained by error propagation. The diamond with error bar shows the experimental result from Ref. [26].

and $b_{2,1}$ are even functions of $E_{\rm ho}/(k_BT)$ [16, 20, 43], and the conjecture of Ref. [25] implies that $b_{3,1}$ and $b_{2,2}$ are also even functions of $E_{\rm ho}/(k_BT)$. Thus, to obtain $b_{3,1}$ and $b_{2,2}$, we fit the data points for the four highest temperatures to the form $a+b[E_{\rm ho}/(k_BT)]^2$. The dashed lines in Figs. 2(a) and 2(b) show the fits. Since the data points at $k_BT = 2E_{\rm ho}$ have much larger error bars than those at lower temperatures, the data points contribute comparatively little to the fit, which weighs each data point by the inverse of the square of its error bar. We find $b^0_{3,1} = 0.0212(8)$ and $b^0_{2,2}/2 = -0.0115(8)$, where the error bars reflect the uncertainty of the fit. We unfortunately do not have sufficiently many data to include a $(k_BT)^{-4}$ term in the fit. Since the inclusion of a $(k_BT)^{-4}$ term in the fit could alter the $T \to \infty$ result, we add an ad-hoc systematic error of 0.0008 to $b^0_{3,1}$ and $b^0_{2,2}/2$, yielding $b^0_{3,1} = 0.0212(16)$ and $b^0_{2,2}/2 = -0.0115(16)$ [crosses in Figs. 2(a) and 2(b)]. To obtain b_4 [see Fig. 2(c)], we combine $b_{3,1}$ and $b_{2,2}$. Specifically, the circles and the fit are obtained by adding the data of Figs. 2(a) and 2(b) while the error bar of the cross at $T \to \infty$ is obtained using standard error propagation. b_4 displays an interesting temperature dependence: It is negative at low temperature due to the dominance of $b_{2,2}$, vanishes at $k_BT \approx E_{\rm ho}$ due to a cancellation of $b_{3,1}$ and $b_{2,2}/2$, and is positive at high temperature due to the dominance of $b_{3,1}$. Our results resolve the discrepancy of the sign of b_4 between Ref. [22] and the experiments [19, 26]. Our extrapolated b_4 at infinite temperature is $b^0_4 = 0.0098(23)$, which agrees with the experimental results of $b^0_4 = 0.01203(125)$ [26] [diamond in Fig. 2(c)] and $b^0_4 = 0.01200(188)$ [19] (see also Table I). Using the LDA, we find $b^{\rm hom}_4 = 0.078(18)$.

We now compare our results for $b^0_{3,1}$ and $b^0_{2,2}$ with the literature. The diagrammatic approach [23] yields $b^0_{3,1} = 0.025$, which is within 2.5 standard deviations of our value, and $b^0_{2,2}/2 = -0.018$, which differs by a factor of about 1.5 (or many standard deviations) from our value. This comparison suggests that the convergence of the diagrammatic approach is slower for the (2,2) system than for the (3,1) system. The conjecture-based approach [24, 25] yields $b^0_{3,1} = 0.02297(4)$, which agrees within error bars with our value, and $b_{2,2}/2 = -0.0309(1)$, which differs by about a factor of 3 from our value.

Conclusion: This letter presented the PIMC determination of the fourth-order virial coefficient of the trapped unitary two-component Fermi gas. Our extrapolated infinite temperature result was found to agree with experiments within error bars, which, to the best of our knowledge, is the first numerical confirmation of the experimental determination of b_4. The customized PIMC scheme, which allows for the treatment of Fermi gases with zero-range interactions, can be applied to a variety of other situations. Since the zero-range density matrix can be constructed for arbitrary s-wave scattering length a_s, the scheme can be used to study the finite-temperature characteristics of the BEC-BCS crossover of few-body Fermi gases. Moreover, the algorithmic developments can be integrated into PIMC ground state calculations, providing a viable alternative to basis set expansion approaches.

Acknowledgement: We are grateful to Kevin M. Daily for valuable correspondence, to Xiangyu Yin for thoughtful comments on the manuscript, and to Yvan Castin for correspondence related to Refs. [25] and [50]. Support by the National Science Foundation (NSF) through Grant No. PHY-1415112 is gratefully acknowledged. This work used the Extreme Science and Engineering Discovery Environment (XSEDE), which is supported by NSF Grant No. OCI-1053575, and the WSU HPC.

Note added: After submission of this paper, Endo and Castin revised their conjecture presented in Ref. [25]. The new calculation yields $b^0_4 = 0.00775(10)$, $b^0_{3,1} = 0.02297(4)$, and $b^0_{2,2}/2 = -0.0152(1)$ [50].

[1] C. J. Pethick and D. G. Ravenhall, "Matter at large neutron excess and the physics of neutron-star crusts," Annu. Rev. Nucl. Part. Sci. **45**, 429 (1995).

[2] P. A. Lee, N. Nagaosa, and X.-G. Wen, "Doping a mott insulator: Physics of high-temperature superconductivity," Rev. Mod. Phys. **78**, 17 (2006).

[3] J. Bardeen, L. N. Cooper, and J. R. Schrieffer, "Microscopic theory of superconductivity," Phys. Rev. **106**, 162 (1957).

[4] R. B. Laughlin, "Anomalous quantum hall effect: An incompressible quantum fluid with fractionally charged excitations," Phys. Rev. Lett. **50**, 1395 (1983).

[5] P. Fulde and R. A. Ferrell, "Superconductivity in a strong spin-exchange field," Phys. Rev. **135**, A550 (1964).

[6] A. Larkin and Y. N. Ovchinnikov, "Nonuniform state of superconductors," Zh. Eksperim. i Teor. Fiz. **47** (1964).

[7] A. Larkin and I. Ovchinnikov, "Inhomogeneous state of superconductors," Soviet Physics-JETP **20**, 762 (1965).

[8] S. Giorgini, L. P. Pitaevskii, and S. Stringari, "Theory of ultracold atomic Fermi gases," Rev. Mod. Phys. **80**, 1215 (2008).

[9] I. Bloch, J. Dalibard, and W. Zwerger, "Many-body physics with ultracold gases," Rev. Mod. Phys. **80**, 885 (2008).

[10] C. Chin, R. Grimm, P. Julienne, and E. Tiesinga, "Feshbach resonances in ultracold gases," Rev. Mod. Phys. **82**, 1225 (2010).

[11] H. Heiselberg, "Fermi systems with long scattering lengths," Phys. Rev. A **63**, 043606 (2001).

[12] T.-L. Ho, "Universal thermodynamics of degenerate quantum gases in the unitarity limit," Phys. Rev. Lett. **92**, 090402 (2004).

[13] K. Huang, *Statistical Mechanics*, 2nd ed. (Wiley, New York, 1987).

[14] T.-L. Ho and E. J. Mueller, "High temperature expansion applied to fermions near Feshbach resonance," Phys. Rev. Lett. **92**, 160404 (2004).

[15] X.-J. Liu, "Virial expansion for a strongly correlated Fermi system and its application to ultracold atomic Fermi gases," Phys. Rep. **524**, 37 (2013).

[16] X.-J. Liu, H. Hu, and P. D. Drummond, "Virial expansion for a strongly correlated Fermi gas," Phys. Rev. Lett. **102**, 160401 (2009).

[17] D. B. Kaplan and S. Sun, "New field-theoretic method for the virial expansion," Phys. Rev. Lett. **107**, 030601 (2011).

[18] X. Leyronas, "Virial expansion with Feynman diagrams," Phys. Rev. A **84**, 053633 (2011).

[19] S. Nascimbene, N. Navon, K. Jiang, F. Chevy, and C. Salomon, "Exploring the thermodynamics of a universal Fermi gas," Nature **463**, 1057 (2010).

[20] Y. Castin and F. Werner, "Le troisième coefficient du viriel du gaz de Bose unitaire," Can. J. Phys. **91**, 382 (2013).

[21] C. Gao, S. Endo, and Y. Castin, "The third virial coefficient of a two-component unitary Fermi gas across an Efimov-effect threshold," Europhys. Lett. **109**, 16003 (2015).

[22] D. Rakshit, K. M. Daily, and D. Blume, "Natural and unnatural parity states of small trapped equal-mass two-component Fermi gases at unitarity and fourth-order virial coefficient," Phys. Rev. A **85**, 033634 (2012).

[23] V. Ngampruetikorn, M. M. Parish, and J. Levinsen, "High-temperature limit of the resonant Fermi gas," Phys. Rev. A **91**, 013606 (2015).

[24] S. Endo and Y. Castin, "Absence of a four-body Efimov effect in the $2+2$ fermionic problem," Phys. Rev. A **92**, 053624 (2015).

[25] S. Endo and Y. Castin, "The interaction-sensitive states of a trapped two-component ideal Fermi gas," (2015), arXiv:1512.06543v1.

[26] M. J. H. Ku, A. T. Sommer, L. W. Cheuk, and M. W. Zwierlein, "Revealing the superfluid lambda transition in the universal thermodynamics of a unitary Fermi gas," Science **335**, 563 (2012).

[27] A. Comtet, Y. Georgelin, and S. Ouvry, "Statistical aspects of the anyon model," J. Phys. A **22**, 3917 (1989).

[28] J. McCabe and S. Ouvry, "Perturbative three-body spectrum and the third virial coefficient in the anyon model," Phys. Lett. B **260**, 113 (1991).

[29] D. M. Ceperley, "Path integrals in the theory of condensed helium," Rev. Mod. Phys. **67**, 279 (1995).

[30] M. Boninsegni, "Permutation sampling in path integral Monte Carlo," J. Low Temp. Phys. **141**, 27 (2005).

[31] Y. Yan and D. Blume, "Incorporating exact two-body propagators for zero-range interactions into N-body Monte Carlo simulations," Phys. Rev. A **91**, 043607 (2015).

[32] L. H. Thomas, "The interaction between a neutron and a proton and the structure of H^3," Phys. Rev. **47**, 903 (1935).

[33] E. Braaten and H.-W. Hammer, "Universality in few-body systems with large scattering length," Phys. Rep. **428**, 259 (2006).

[34] D. S. Petrov, "Three-body problem in Fermi gases with short-range interparticle interaction," Phys. Rev. A **67**, 010703 (2003).

[35] G. V. Skorniakov and K. A. Ter-Martirosian, "Three body problem for short range forces. I. Scattering of low energy neutrons by deuterons," Zh. Eksp. Teor. Fiz. **31**, 775 (1956), [Sov. Phys. JETP **4**, 648 (1957)].

[36] M. Takahashi and M. Imada, "Monte Carlo calculation of quantum systems," J. Phys. Soc. Japan **53**, 963 (1984).

[37] D. M. Ceperley, "Path integral Monte Carlo methods for fermions," in *The Proceedings of the Les Houches Summer School, Session 56, Strongly Interacting Fermions and High T_c Superconductivity*, edited by B. Doucot and J. Zinn-Justin (Elsevier, Amsterdam, 1995) p. 427.

[38] E. Y. Loh, J. E. Gubernatis, R. T. Scalettar, S. R. White, D. J. Scalapino, and R. L. Sugar, "Sign problem in the numerical simulation of many-electron systems," Phys. Rev. B **41**, 9301 (1990).

[39] R. Stratonovich, "On a method of calculating quantum distribution functions," Sov. Phys. Dokl. **2**, 416 (1957).

[40] D. Ceperley and B. Alder, "Quantum Monte Carlo," Science **231**, 555 (1986).

[41] K. Huang and C. N. Yang, "Quantum-mechanical many-body problem with hard-sphere interaction," Phys. Rev. **105**, 767 (1957).

[42] X.-J. Liu and H. Hu, "Virial expansion for a strongly correlated Fermi gas with imbalanced spin populations," Phys. Rev. A **82**, 043626 (2010).

[43] K. M. Daily and D. Blume, "Thermodynamics of the two-component Fermi gas with unequal masses at unitarity," Phys. Rev. A **85**, 013609 (2012).

[44] The explicit expressions for $b^{\rm ref}_{n_1,n_2}$ with $n_1+n_2=4$ read $b^{\rm ref}_{3,1}=-b_3Q_{1,0}-2b_2Q_{2,0}$ and $b^{\rm ref}_{2,2}=-2b_3Q_{1,0}-2(b_2)^2Q_{1,0}-2b_2(Q_{1,0})^2$.

[45] The supplemental material at TO.BE.INSERTED.BY.THE.EDITOR contains (i) a summary of the literature values of the fourth-order virial coefficient; (ii) information on the pair product approximation and the two-body density matrix for zero-range interactions; and (iii) PIMC simulation details and tables containing selected raw data.

[46] For a simulation of finite length l, the standard deviation would not be following a Gaussian distribution, implying that the standard deviation would not decrease as $1/\sqrt{l}$ with increasing simulation length l.

[47] For the (2,2) system, e.g., $\mathcal{A}$ reads $(1-P_{12}-P_{34}+P_{12}P_{34})/4$, where P_{ij} permutes the coordinates of particles i and j.

[48] S. A. Chin, "High-order path-integral Monte Carlo methods for solving quantum dot problems," Phys. Rev. E **91**, 031301(R) (2015).

[49] Y. Yan and D. Blume, "Temperature dependence of small harmonically trapped atom systems with Bose, Fermi, and Boltzmann statistics," Phys. Rev. A **90**, 013620 (2014).

[50] S. Endo and Y. Castin, "The interaction-sensitive states of a trapped two-component ideal Fermi gas and application to the virial expansion of the unitary Fermi gas," (2016), arXiv:1512.06543v2.

arXiv:1602.02328v2 [cond-mat.quant-gas] 12 May 2016

Supplemental Material

Path integral Monte Carlo determination of the fourth-order virial coefficient for unitary two-component Fermi gas with zero-range interactions

Yangqian Yan[1] and D. Blume[1]

[1] *Department of Physics and Astronomy, Washington State University, Pullman, Washington 99164-2814, USA*

(Dated: May 13, 2016)

The notation employed in this Supplemental Material follows that introduced in the main text.

I. LITERATURE VALUES OF b_4

Table S1 summarizes the literature results for the fourth-order virial coefficient; this table is an extended version of Table I of the main text. The non-interacting contribution to the total fourth-order virial coefficient $b_4^{\rm hom,tot}$ of the homogeneous system is given by

$$b_n^{\rm hom,ni} = (-1)^{n+1}/n^{5/2}; \tag{S1}$$

the interacting part of the fourth-order virial coefficient $b_4^{\rm hom}$ of the homogeneous system is defined through

$$b_n^{\rm hom} = b_n^{\rm hom,tot} - b_n^{\rm hom,ni}. \tag{S2}$$

TABLE S1. Summary of literature results. The value reported in the respective reference is underlined. The conversion to other "representations" is done using Eqs. (S1)-(S3). The column labeled "Ref." refers to the bibliography of the main text.

$b_4^{\rm hom}$	$b_4^{\rm hom,tot}$	b_4^0	Ref.	comment
<u>0.096(15)</u>	0.065(15)	0.01200(188)	19	ENS experiment
0.096(10)	<u>0.065(10)</u>	0.01203(125)	26	MIT experiment
-0.016(4)	-0.04725(40)	<u>-0.0020(5)</u>	22	sum-over-states approach
<u>0.06</u>	0.02875	0.0075	23	diagrammatic approach
<u>-0.063(1)</u>	-0.09425(10)	-0.007875(125)	24	3-body inspired conjecture

The interacting part of the fourth-order virial coefficient b_4^0 of the harmonically trapped system at high temperature and $b_4^{\rm hom}$ are related via (see also the main text),

$$b_n^{\rm hom} = n^{3/2} b_n^0. \tag{S3}$$

II. PAIR PRODUCT APPROXIMATION AND ZERO-RANGE DENSITY MATRIX

Equation (9) of the main text writes the observable $Q^{\rm ni}_{n_1,n_2}/Q_{n_1,n_2}$ in terms of the density matrices $\rho^{\rm ni}(\mathbf{R}_i, \mathbf{R}_{i+1}; \tau)$ and $\rho(\mathbf{R}_i, \mathbf{R}_{i+1}; \tau)$ of the non-interacting and unitary (n_1, n_2)-particle systems. To evaluate the density matrix by the PIMC approach, we use the pair product approximation [1],

$$\rho(\mathbf{R}, \mathbf{R}'; \tau) \approx \left(\prod_{j=1}^{n_1+n_2} \rho^{\rm sp}(\mathbf{r}_j, \mathbf{r}'_j; \tau) \right) \times \left(\prod_{j=1}^{n_1} \prod_{k=n_1+1}^{n_1+n_2} \bar{\rho}^{\rm rel}(\mathbf{r}_j - \mathbf{r}_k, \mathbf{r}'_j - \mathbf{r}'_k; \tau) \right), \tag{S4}$$

where $\rho^{\rm sp}(\mathbf{r}, \mathbf{r}'; \tau)$ is the single-particle density matrix [1],

$$\rho^{\rm sp}(\mathbf{r}, \mathbf{r}'; \tau) = a_{\rm ho}^{-3} \left[2\pi \sinh(\tau\hbar\omega)\right]^{-3/2} \times \exp\left(-\frac{(\mathbf{r}^2 + \mathbf{r}'^2)\cosh(\tau\hbar\omega) - 2\mathbf{r}\cdot\mathbf{r}'}{2\sinh(\tau\hbar\omega) a_{\rm ho}^2} \right), \tag{S5}$$

and $\bar{\rho}^{\rm rel}(\mathbf{r}, \mathbf{r}'; \tau)$ is the reduced pair density matrix of the relative two-body problem with zero-range interaction [2],

$$\bar{\rho}^{\rm rel}(\mathbf{r}, \mathbf{r}'; \tau) = 1 + \frac{2\hbar^2\tau}{mrr'} \exp\left(-\frac{m(rr' + \mathbf{r}\cdot\mathbf{r}')}{2\hbar^2\tau} \right). \tag{S6}$$

The density matrix $\rho^{\rm ni}$ of the non-interacting system is given by Eq. (S4) with $\bar{\rho}^{\rm rel}$ replaced by 1.

III. EXTRAPOLATION TO THE $\tau \to 0$ LIMIT AND SELECTED RAW DATA

As mentioned in the main text, to determine b_n with comparable percentage accuracy at all temperatures, $Q^{\rm ni}_{n_1,n_2}/Q_{n_1,n_2}$ has to be determined with increasing percentage accuracy with increasing temperature. To ensure that our results are free of systematic errors, the error introduced by the $\tau \to 0$ extrapolation has to be smaller than the error of the extrapolation that arises from the statistical error of the individual PIMC data points. To illustrate this, we consider the (2,1) system at the highest temperature considered, i.e., at $k_B T = 2E_{\rm ho}$.

Circles in Fig. S1(a) show $Q^{\rm ni}_{2,1}/Q_{2,1}$, obtained by our PIMC approach, as a function of the imaginary time step τ (the data correspond to $N = 2, 3, 4$, and 6). The solid line shows a fourth-order fit of the form $a + b\tau^2 + c\tau^4$ to our

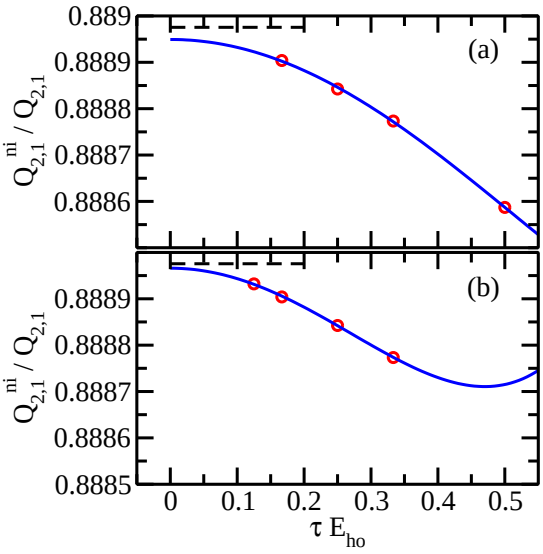

FIG. S1. (Color online) Benchmarking our PIMC results (circles) for the (2,1) system at unitarity through comparison with sum-over-states results. The observable $Q^{\rm ni}_{2,1}/Q_{2,1}$ as a function of the imaginary time step τ at temperature $k_BT = 2E_{\rm ho}$. The error bars (not shown) are smaller than the symbol size. In (a), the time steps correspond to $N = 2$, 3, 4, and 6. In (b), the time steps correspond to $N = 3$, 4, 6, and 8. The solid line shows the fourth-order polynomial fit of the form $a + b\tau^2 + c\tau^4$. The dashed line shows the sum-over-states results.

PIMC data. The extrapolated $\tau \to 0$ value of 0.888949(8), where the error bar accounts for the statistical uncertainty of the PIMC data, deviates by about 3 standard deviations (or 0.003%) from the sum-over-states result of 0.8889755. We attribute the discrepancy to the fact that the τ considered are not small enough for the fourth-order fit to be fully reliable. To corroborate this interpretation, we (i) employ a sixth-order fit and (ii) apply the fourth-order fit to PIMC data for smaller τ. The sixth-order fit (using, as before, the data corresponding to $N = 2, 3, 4$, and 6) yields 0.888964(19), in agreement with the sum-over-states result. Note, however, that the error bar is much larger than that resulting from the fourth-order fit; the reason is that we are attempting to determine four fit parameters using just four data points. Performing a fourth-order fit to the PIMC data for $N = 3, 4, 6$, and 8 yields 0.888966(8), which almost agrees with the sum-over-states approach within error bar and with an error bar that is comparable to our previous fourth-order fit [see Fig. S1(b)]. This analysis suggests that our PIMC calculations are free of systematic errors provided we go to sufficiently small τ.

Table S2 lists the PIMC raw data for the (3,1) and (2,2) systems at various temperatures (the data for low temperatures are not shown). We report the observables $Q^{\rm ni}_{3,1}/Q_{3,1}$ and $Q^{\rm ni}_{2,2}/Q_{2,2}$ for various time slices. For $E_{\rm ho}/(k_BT) = 0.6$, 0.7, and 0.8, the largest number of time slices considered is $N_{\rm max} = 9$. For $E_{\rm ho}/(k_BT) = 0.5$, our

TABLE S2. Selected PIMC raw data. Columns 1 and 2 show the inverse temperature $E_{\rm ho}/(k_BT)$ and the number of imaginary time slices N, respectively. Columns 3 and 4 show the observables $Q^{\rm ni}_{3,1}/Q_{3,1}$ and $Q^{\rm ni}_{2,2}/Q_{2,2}$ for the (3,1) and (2,2) systems, respectively.

$E_{\rm ho}/(k_BT)$	N	$Q^{\rm ni}_{3,1}/Q_{3,1}$	$Q^{\rm ni}_{2,2}/Q_{2,2}$
0.5	2	0.8413081(35)	0.7940517(46)
0.5	3	0.8418155(43)	0.7946990(43)
0.5	4	0.8420157(41)	0.7949482(45)
0.5	6	0.8421806(41)	0.7951732(53)
0.6	3	0.754475(16)	0.686274(11)
0.6	4	0.754955(12)	0.686860(11)
0.6	5	0.755218(12)	0.687174(14)
0.6	7	0.755450(13)	0.687445(14)
0.6	9	0.755591(15)	0.687587(14)
0.7	3	0.658547(24)	0.571429(24)
0.7	4	0.659464(22)	0.572473(14)
0.7	6	0.660203(26)	0.573329(22)
0.7	9	0.660583(29)	0.573764(23)
0.8	4	0.563935(34)	0.462752(36)
0.8	5	0.564662(35)	0.463530(33)
0.8	7	0.565379(36)	0.464433(32)
0.8	9	0.565708(38)	0.464757(33)

available computing resources limit us to $N_{\rm max} = 6$, resulting in reduced accuracy of the observables.

For $E_{\rm ho}/(k_BT) = 0.6$, 0.7, and 0.8, we perform fourth-order fits to the τ-dependent $Q^{\rm ni}_{3,1}/Q_{3,1}$ and $Q^{\rm ni}_{2,2}/Q_{2,2}$ data listed in Table S2, yielding extrapolated $\tau \to 0$ values with error bars between 0.0024% and 0.016%. We estimate, based on our tests for the three-body system, that these statistical errors are larger than the systematic error, which arises from the use of the fourth-order fit. Hence the systematic uncertainty can be neglected. For $E_{\rm ho}/(k_BT) = 0.5$, a fourth-order fit to the data given in Table S2 yields error bars of 0.0008% and 0.001% for $Q^{\rm ni}_{3,1}/Q_{3,1}$ and $Q^{\rm ni}_{2,2}/Q_{2,2}$, respectively. Since we estimate the systematic fit uncertainty to be, based on our analysis for the (2,1) system, about 0.003%, we deem the fourth-order fit unreliable. Using a sixth-order fit (which yields a larger error bar), we find the

TABLE S3. Selected extrapolated PIMC results. Columns 1 and 2 show the inverse temperature $E_{\rm ho}/(k_BT)$ and the order used in the extrapolation, respectively. Columns 3 and 5 show the extrapolated $\tau \to 0$ observables $Q^{\rm ni}_{3,1}/Q_{3,1}$ and $Q^{\rm ni}_{2,2}/Q_{2,2}$ for the (3,1) and (2,2) systems, respectively. Columns 4 and 6 show the resulting subcluster contributions $b_{3,1}$ and $b_{2,2}/2$, respectively, to the fourth-order virial coefficient.

$E_{\rm ho}/(k_BT)$	order	$Q^{\rm ni}_{3,1}/Q_{3,1}$	$b_{3,1}$	$Q^{\rm ni}_{2,2}/Q_{2,2}$	$b_{2,2}/2$
0.5	6	0.842330(15)	0.0194(16)	0.795393(18)	−0.0139(16)
0.6	4	0.755751(18)	0.0153(4)	0.687775(18)	−0.0102(4)
0.7	4	0.660877(39)	0.0135(3)	0.574108(30)	−0.0095(2)
0.8	4	0.566227(82)	0.0111(2)	0.465415(73)	−0.0093(2)

values listed in Table S3.

[1] D. M. Ceperley, "Path integrals in the theory of condensed helium," Rev. Mod. Phys. **67**, 279 (1995).

[2] Y. Yan and D. Blume, "Incorporating exact two-body propagators for zero-range interactions into N-body Monte Carlo simulations," Phys. Rev. A **91**, 043607 (2015).